Fabrication and characterization of a new high density Sc/Si multilayer sliced grating

Dmitriy L. Voronov,[a*] Rossana Cambie,[a] Eric M. Gullikson,[a] Valeriy V. Yashchuk,[a]
Howard A. Padmore,[a] Yuri P. Pershin,[b] Alexander G. Ponomarenko,[b] Valeriy V. Kondratenko[b]
[a] Advanced Light Source, Lawrence Berkeley National Laboratory, Berkeley, California, 94720
[b] National Technical University "KhPI", Kharkov, Ukraine, 61002

ABSTRACT

State of the art soft x-ray spectroscopy techniques like Resonant Inelastic X-ray Scattering (RIXS) require diffraction gratings which can provide extremely high spectral resolution of 10^5-10^6. This problem may be addressed with a sliced multilayer grating with an ultra-high groove density (up to 50,000 mm^{-1}) proposed in the recent publication [Voronov, D. L., Cambie, R., Feshchenko, R. M., Gullikson, E., Padmore, H. A., Vinogradov, A. V., Yashchuk, V. V., Proc. SPIE 6705, 67050E (2007)]. It has been suggested to fabricate such a grating by deposition of a soft x-ray multilayer on a substrate which is a blazed saw-tooth grating (echellette) with low groove density. Subsequent polishing applied to the coated grating removes part of the coating and forms an oblique-cut multiline structure that is a sliced multilayer grating. The resulting grating has a short-scale periodicity of lines (bilayers), which is defined by the multilayer period and the oblique-cut angle. We fabricated and tested a Sc/Si multilayer sliced grating suitable for EUV applications, which is a first prototype based on the suggested technique. In order to fabricate an echellette substrate, we used anisotropic KOH etching of a Si wafer. The etching regime was optimized to obtain smooth and flat echellette facets. A Sc/Si multilayer was deposited by dc-magnetron sputtering, and after that it was mechanically polished using a number of diamond pastes. The resulting sliced grating prototype with ~270 nm line period has demonstrated a dispersive ability in the 41-49 nm photon wavelength range with a diffraction efficiency of ~7% for the optimized 38th order assigned to the echellette grating of 10 µm period.

Keywords: resonant inelastic X-ray scattering, high density grating, anisotropically etched silicon gratings, soft x-ray multilayers, sliced multilayer grating, spectral resolution, RIXS

1. INTRODUCTION

Development of high resolution diffraction gratings for the EUV and soft x-ray energy ranges is one of the major challenges for modern astronomy[1,2] as well as for precision spectroscopy being carrying out at synchrotron facilities around the world.[3,4] A relatively new and extremely exciting development of high resolution soft x-ray spectroscopy is a method of Resonant Inelastic X-ray Scattering (RIXS) that potentially allows to directly measure the energies of the soft excitations of correlated electronic systems such as high T_c superconductors (for review, see Refs.[5-7] and references therein). However, in order to realize the potential of the method, a dedicated spectrometer must achieve energy resolution of ~10 meV in the 100-eV to 5-keV photon energy range[4] that corresponds to resolving powers up to 100 times that achieved now.

There are two principle ways to achieve ultra-high spectral resolution in the soft X-ray wavelength range. One way is to use high order diffraction with a grating with reasonably low groove density, while another one is to use the first order diffraction of a grating with an ultra-high density of grooves. A conventional grating, if it is used for high order x-ray diffraction, would provide very low diffraction efficiency, because for all normal reflecting materials, the scattering angle would need to be bigger than the critical angle of the material. The effective critical angle can be significantly increased with a multilayer (ML) coating.[8,9] In this case, the Bragg equation for the multilayer and the high order diffraction equation for the surface grating have to be simultaneously fulfilled. By choosing the appropriate set of multilayer and grating period parameters, it becomes possible to maximize diffraction efficiency for a selected high order. The lamellar ML grating,[10-12] blazed ML grating,[14-17] and sliced ML grating[18,19] are the examples of such a grating. The best result that has been demonstrated with a grating with a multilayer reflecting coating[17] was obtained with a grating with an echellette[20] substrate.

A number of methods have been developed to fabricate an echellette grating. For example, a method discussed in Ref.[1] uses an argon and oxygen mixed-gas ion beam to directly etch the grating substrate through a rectangular profile photoresist grating mask. A holographic ion-etched spherical blazed grating and three of its fourth-generation replicas are described in Refs.[2] A limiting factor of the methods is a significant roughness of the echellette facets that leads to degradation of grating efficiency due to growing perturbation of the interlayer boundaries. Higher surface quality of the echellette facets has been obtained with anisotropic etching of an asymmetrically cut Si {111} crystal. The method was first used in Ref.[21] and brought to the state of the art level in work at MIT,[16,22] where the saw-like groove density of ~5000 lines per millimeter has been achieved.

Aiming for a resolving power in first order diffraction order of 10^6 in a reasonably compact x-ray spectrometer assumes the need for 10^6 grating grooves with extremely high line density, ~50,000 l/mm. For high energy x-ray applications, there is a unique opportunity to use an asymmetrically cut crystal as a ultra-high density grating.[23-25] Unfortunately, it is difficult, if not impossible, to find a crystal with the large enough lattice constant, which is for soft x-ray applications.[26]

A grating with very small period, suitable for EUV wavelength range, has been fabricated by slicing and polishing the $MoSi_2$/Si multilayer structure at 10º angle to the plane of the multilayer.[18,19] This reveals the periodic bilayer structure with the period determined by the values of the multilayer period and slice angle. The grating equation and Bragg condition are fulfilled simultaneously, so the highest diffraction efficiency of the grating is achieved in first order, while the Bragg condition for the first order reflection from the ML structure is satisfied. In spite of the fact that a high dispersive power of the grating fabricated this way was experimentally demonstrated,[18,19] the total resolution that is the number of bilayers is difficult to exceed 10^3 due to limitations of the deposition technique (see analysis in Ref.[27]).

At the ALS Experimental Systems Group (ESG) in fiscal year 2007, an LDRD (Laboratory Directed Research and Development) project to establish and demonstrate the technology required for ultra-high resolution RIXS with soft x-rays has been started. In the scope of the project, a technique to fabricate a required high-density grating based on cutting at an oblique angle a small period multilayer mirror deposited on an echellette substrate has been suggested.[27] Fabrication of such a grating for ultra-high resolution spectroscopy with soft x-rays is a challenging problem itself.

In this article, we present an overview of recent efforts on fabrication and characterization of a high density sliced Sc/Si multilayer grating that is a proof of principle realization of the fabrication method suggested in Ref.[27] With groove density of ~3700 lines per mm, the grating prototype is suitable for EUV applications. Although the groove density is smaller than that required for ultra-high resolution spectroscopy with soft x-rays, the prototype grating is rather convenient for characterization with a number of techniques, including scanning probe, electron, and interferometric microscopy. This allows checking the consistency of the approaches proposed, as well as optimizing the grating fabrication technology.

The structure of the article is as follows. In the next section, we discuss the essential elements of fabrication of a sliced multilayer grating with an echellette substrate. In Sec. 3, the results of diffraction measurements with the EUV grating prototype with sliced Sc/Si multilayer are presented. The measurements were performed at the ALS beam line 6.3.2. Directions for further investigations are outlined in the Conclusion.

2. FABRICATION OF SLICED MULTILAYER GRATINGS

2.1 Design conception: three steps of grating fabrication

Figure 1 illustrates the sequential processes to fabricate a high density multilayer sliced grating. The fabrication includes three major steps depicted in Fig. 1.

a) anisotropically etched Si grating   b) multilayer coated echellette   3) multilayer sliced grating
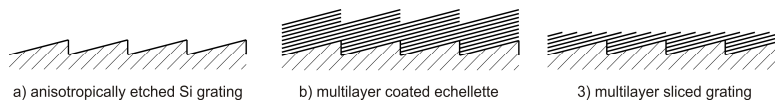
Figure 1: Sequential processes to fabricate a high density multilayer sliced grating: a) a saw-tooth-shaped grating (echellette) is created; b) a high reflectivity multilayer is deposited on the echellette; c) the multilayer coating is sliced at a small angle by chemical/mechanical polishing.

First (Fig. 1a), a relatively low resolution saw-tooth-shaped grating (echellette) is created. Currently in this step, we use anisotropic etching of an asymmetrically cut Si {111} crystal. Second (Fig. 1b), a high reflectivity multilayer, optimized for a certain photon energy range, is deposited on the echellette. For the grating prototype described throughout the

present work, Sc/Si multilayers of total number of 40 bilayers (overall multilayer thickness was about 1 µm) were deposited onto a 10-µm-period 6-degree-blaze-angle echellette using a dc-magnetron sputtering technique. At the same time and conditions, a flat silicon witness was also coated. The witness was to be used for a control measurement of the multilayer reflectivity. And third (Fig. 1c), the multilayer coating is sliced at a small angle by a chemically/mechanically polishing. The peculiarities of the involved processes are discussed below.

2.2 Anisotropic etching of Si wafer

The process of anisotropic etching of a Si {111} crystal with an aqueous solution of potassium hydroxide, KOH, was optimized in order to fabricate a high quality echellette grating with relatively low groove density. The parameters (grating period of 10 µm and blaze angle of 6 degrees) of the grating used for the optimization experiments were chosen from the point of view of convenience of characterization of the etched surfaces and structures with the available instruments: a scanning electron microscope (SEM), a scanning probe microscope (SPM), and an interferometric microscope. We use {111} Si wafers with 6 degree inclination of the surface plane from the {111} crystal plane towards either direction $\langle \bar{1}\,\bar{1}\,2 \rangle$, or direction $\langle 11\bar{2} \rangle$ as the material for echellette fabrication. Wafers made of float zone (FZ) Si crystals and crystals grown by the Czochralski process (CZ) were used. Before etching in KOH, a low stress silicon nitride layer was first deposited onto the wafer. Then a grating pattern was printed on the nitride by contact lithography and reactive ion etching.

Figure 2 shows the SEM images of the echellette gratings etched on Si wafers with different inclinations of the surface plane from {111} crystal plane: towards direction $\langle \bar{1}\,\bar{1}\,2 \rangle$ - Fig. 2b, and towards direction $\langle 11\bar{2} \rangle$ - Fig. 2c. The nitride mask is seen on the tops of the Si nubs in Fig. 2b. The nitride mask is removed after etching is complete.
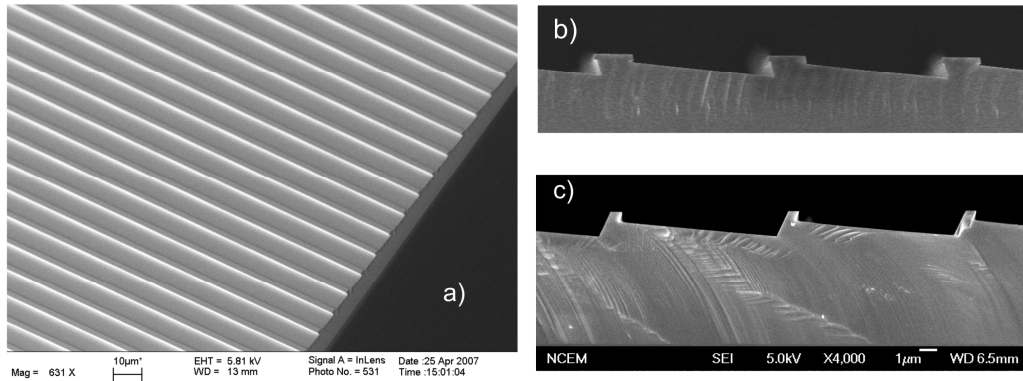

Figure 2: SEM images of the echellette gratings fabricated by anisotropic etching of Si [CZ for a) and b) and FZ for c)] wafers with aqueous KOH: a) top view of a grating with period of 10 microns and the blaze angle of 6 degrees; b) and c) profiles of similar gratings made of a Si wafer with 6 degree inclination of the surface plane from the {111} crystal plane towards direction $\langle \bar{1}\,\bar{1}2 \rangle$ and towards direction $\langle 11\bar{2} \rangle$, respectively.

Surface morphology (via 2 dimensional surface height distributions) of an echellette grating facet measured with the SPM is shown in Fig. 3. Figures 3a and 3b correspond to a grating that was etched in 20% aqueous KOH at room temperature. Figure 3c represents a grating additionally etched for 20 minutes in ammonium fluoride (NH$_4$F). The same scan is shown in Figs. 3a and 3b, but for Fig. 3b the measured height distribution was detrended in such a way that {111} terrace planes are parallel to the image plane, rather than a plane surface detrending over the distribution, which was applied to plot Fig. 3a.

After KOH etching (Figs. 3a and 3b), the facet surface consists of atomically smooth {111} terraces, atomic steps, and pits on terraces. Such morphology is characteristic for the step-flow mechanism of KOH anisotropic etching.[28-30] The facet surface roughness measured over 1×1 µm^2 area was achieved to be ~2.6 Å (rms). The value of the roughness is determined by anisotropy of site specific etch rates for terraces (i. e. probability of removal of a silicon atom out of a {111} plane) and steps (i. e. probability of removal of an atom from a step). The achieved facet roughness of 2.6 Å (rms) is larger than that of a polished wafer used (~1 Å), but significantly smaller than the roughness of ~5.6 Å obtained for an echellette grating fabricated with holographic ion-etching.[2]
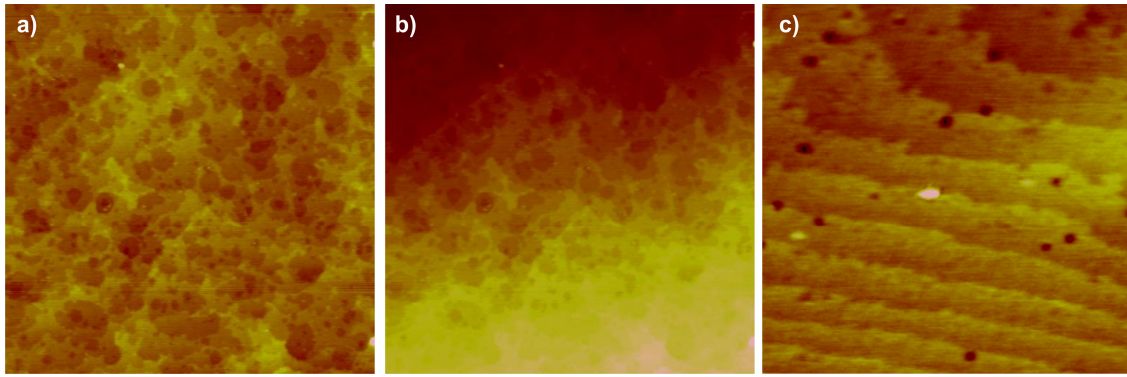
Figure 3: a), b) SPM images of the surface height distribution of a facet of an echellette grating etched from a CZ wafer in 20% aqueous KOH at room temperature; c) similar image but of a grating made of a FZ wafer with the same KOH etching and after that additionally etched for 20 minutes in NH_4F at room temperature. Images a) and b) show the same height distribution but differently detrended – see text. The size of the scanned areas is 1×1 μm^2. In the course of the SPM measurements shown, the echellette grooves were oriented horizontally with the deeper side at the bottom of the images.

One of the straightforward ways to improve smoothness of the grating facets is to use an etchant with a higher anisotropy of etching of steps and terraces. For this purpose, we have used ammonium fluoride that is known to have a significantly higher anisotropy of etching of Si than KOH. After the KOH etching, an additional etching in ammonium fluoride for 20 min at room temperature allowed us to improve the facet surface roughness to ~1.1 Å (rms) - Fig. 3c. Note, that the etching in NH_4F is not yet optimized. We are working on the optimization.

After NH_4F etching, the facet surface morphology (Fig. 3c) is noticeably modified and looks now as a set of extended atomically smooth terraces with steps of the same sign, regularly distributed across a facet. As a result the facet surface deviates from the {111} crystal plane. The deviation can be an inherent property of the anisotropic etching of an asymmetrically cut Si crystal. In this case, there is a difference in time of exposition with the etchant for the upper and the bottom parts of a facet. As a result, a new step can appear on a terrace plane formed on the upper part of a facet, when the bottom part of the same plane still remains buried. Such a step will propagate down to the bottom part of the facet. In this model, the value of the deviation is inversely proportional to the anisotropy of etching and stays constant (with a constant declination angle) along the facet.

However, in Fig. 3c, the atomic steps are distributed non-uniformly (step density higher on the bottom part of a facet) suggesting that anisotropy of the etching significantly varies along a facet. The non-uniformity leads to a curved facet that is clearly seen in Fig. 4, where a profile of an echellette groove is shown. The concave shape of the facets is consistent with assumption of an autocatalytic nature of etching chemical reactions,[28] which can also explain the variation across a facet, the anisotropy of etching mentioned above. Note, that the 30-min long NH_4F etching applied so far is probably too short in order to significantly effect the overall shape of the grating facets.
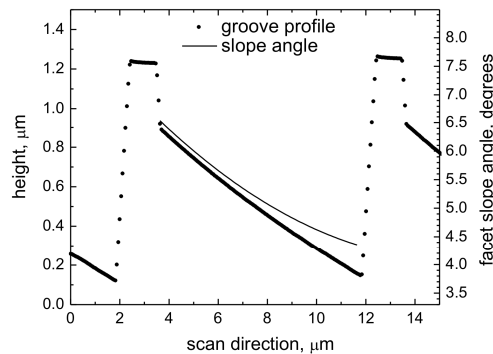

Figure 4: Profile of a grating groove measured with the SPM. The grating was etched for 4 hours in 20% KOH at room temperature. The curved shape of the facet reproduces the variation of the terrace sizes across a facet in Fig. 3c.

We have observed that the average density of the steps decreases and distribution of the steps becomes more uniform with increased etching time. Accordingly, the facet curvature is also decreased. However, longer etching leads to other severe defects on the facet surface. These are the micron-scaled conical pits – Fig. 5. Diameter of the pits can be 10-20 µm with a depth of tens of nanometers. The slope angle of the generating lines of the pit cones was measured to be within a narrow range between 0.5 and 1 degrees, depending on etching parameters.
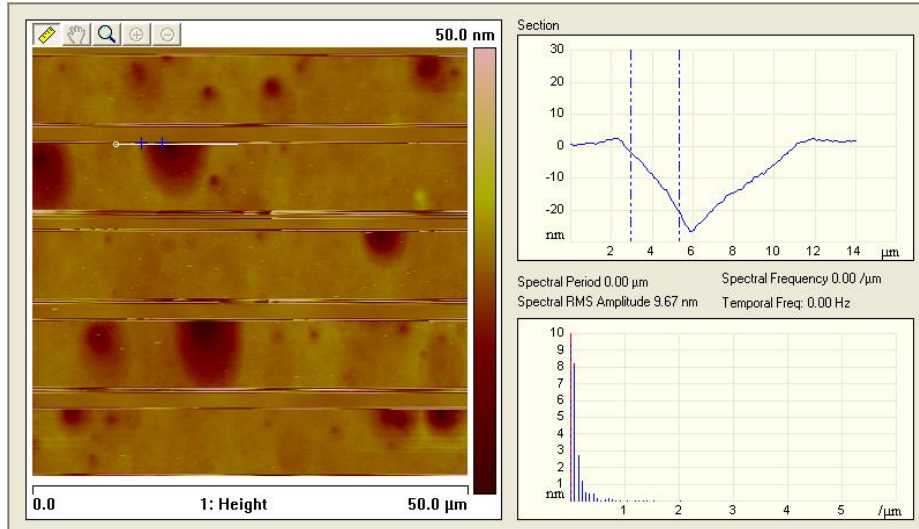
Figure 5: Conical pits on the facet surface of an echellette etched for in 20% KOH at ~25C on a CZ wafer.

Nucleation of pits is usually ascribed to a high oxygen content in a CZ wafer.[29,30] We have etched at the same conditions (20% KOH at ~23K with a magnetic bar steering) the CZ and FZ wafers with the specified concentration of oxygen of 20 ppm and <1 ppm, respectively. In spite of the fact that the resulting surface quality for the FZ wafer was better, we cannot reliably conclude that in our case oxygen contamination in the initial material is a dominating factor for pit formation. Note, that the wafers also differed in the direction of the 6 degree inclination.

Among other possible reasons for pit formation, contamination of Si surface with some particles (O_2, metal atoms, solid reaction products, etc.) in the course of etching is most probable. Figure 6 provides a clue to a presence of a particle in the centre of a pit seen in the amplitude signal image obtained with the SPM.
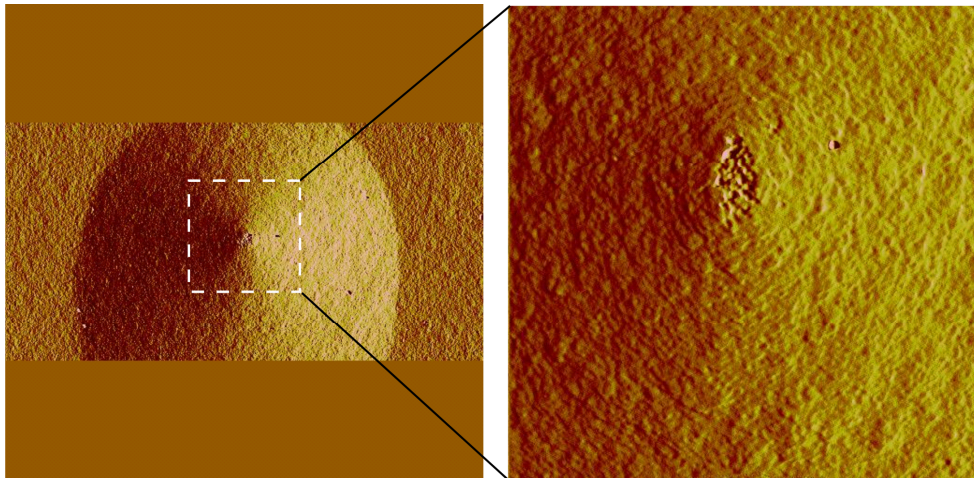

Figure 6: Conical pit on the surface of a facet as it is reproduced with the SPM in the amplitude signal image. The size of the exaggerated area is about 1×1 µm². There is an obvious discontinuity at the pit's center. It can be a manifestation of a foreign particle.

Unfortunately, a measurement, such as one in Fig. 6, does not allow us to reliably conclude anything about the physical meaning of the observation. But in any case, we found the situation shown in Fig. 6, where there is an obvious perturbation in the center of a pit, to be rather typical. The perturbation is probably responsible for a local, near the pit center, decrease of etching anisotropy. The decrease of etching anisotropy manifests itself via a roll off of the pit cone generating lines observed in pit cross-section near the pit center; see Fig. 5. Due to the perturbation, the probability for formation of a new step on the lower terraces of a pit is higher at the pit center; whereas for the rest of the pit, the etching anisotropy is constant and can be numerically characterized via an asymptotic slope of the generating lines.

The assumption about a relation between shape of a pit and etching anisotropy can be modeled in a simple way illustrated in Fig. 7.
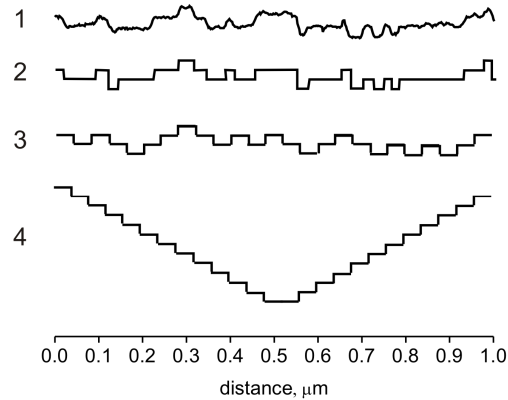

Figure 7: Sketch to illustrate the suggested mechanism of formation of a conical pit and to explain a relation between shape of a pit and anisotropy of etching.

In Fig. 7, the line 1 is a measured surface profile of a facet (compare with Fig. 3a). On the profile, one can sight multiple terraces that involve only four {111} atomic planes. The line 2 is an approximation of the profile shown with the line 1, but now the terraces and steps have an ideally flat shape. The 1-µm long trace 2 consists of total 25 atomic steps that include 12 upward and 13 downward steps. The averaged width of a terrace is ~40 nm. This value is used for transformation of the line 2 to the line 3. Finally, using an assumption about a larger probability of pit formation at the center (but ignoring a change of the etching anisotropy), the steps of the opposite directions are separated, reproducing a shape of a pit etched at the same conditions. The corresponding slope angle found to be about 0.5 degrees is in a good agreement with the facet declination angle in respect to the {111} plane that, we think, also relates to the value of anisotropy of KOH etching.

Note that pit nucleus with an ideal shape, as one shown in Fig. 7 with the line 4, become stable and cannot be removed with continuing of etching. It relates to an observation[30] that probability of pit formation on a surface near parallel to a {111} plane has a strong dependence on the delineation angle. At a surface declination angle larger than the angle characteristic for the slope of the tip generating lines, nucleation of a new tip becomes impossible.

Due to the pit stabilization effect, a fluctuation mechanism of pit formation on a {111} plane is also possible. In this case, fluctuation of positions of new steps can lead to the appearance of a pit with a size large enough for triggering of the stabilization effect. Because of longer etching time and smaller declination angle, pits start first to grow in the upper part of the grating facets. Therefore, one of the parameters of the etching process to be optimized is an optimal etching time, short for the pits to start to actively grow up and long enough to provide completed smooth facets.

We have chosen to stop KOH etching as soon as the first pit nuclei appear. This situation is depicted in Fig. 8, where surface morphology of an echellette grating, fabricated with KOH etching with all other parameters also optimized, is shown. The optimization allowed us to obtain an echellette with the facet surface with a wide bandwidth roughness (measured over an area of $20 \times 6 \ \mu m^2$ area) of ~5 Å (rms). A major contribution to the roughness gives a residual waviness of the grating facets clearly seen in Fig. 8. We believe that the waviness originates from the defects of the lithographic mask we used, rather than from the KOH etching itself. The waviness remains a serious problem, and we are working to solve it.
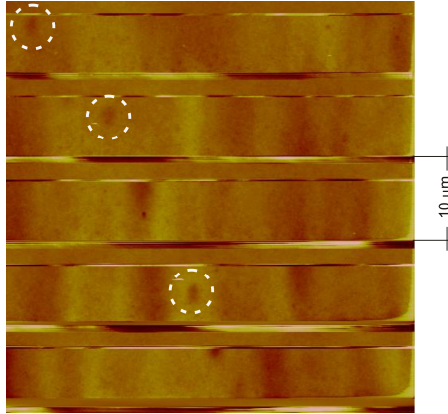
Figure 8: Surface morphology of a 50 µm × 50 µm area of an echellette grating fabricated with KOH etching with optimized parameters (see text). Practically, on the scanned area, there is not a self-evident pit. However, there are a few marks (depicted with the circles) of pit nucleation. The residual waviness of a facet gives the major contribution to the value of the wide bandwidth surface roughness that was measured over a 20 µm × 6 µm area to be ~5 Å (rms).

2.3 Deposition of Sc/Si multilayer coating on an echellette grating and finishing polishing

In experiments on the deposition of a Sc/Si multilayer coating we have used a number of echellette samples made of CZ and FZ crystals with different directions of the 6 degree inclination. For the prototype grating described below, Sc/Si multilayers of total number of 40 bilayers (the total thickness of the multilayer coating was about 1 µm) were deposited onto a 10-µm-pitch 6-degree-blaze-angle echellette with dc-magnetron sputtering. We used a FZ wafer with 6 degree inclination of the surface plane from the {111} crystal plane towards direction $\left\langle \bar{1}\,\bar{1}\,2 \right\rangle$. At the same time and conditions, a flat silicon witness was also coated. The witness was used for a control measurement of the multilayer reflectivity.

Figure 9 shows the SEM images of a cross-section of an echellette grating covered with the Sc/Si multilayer. In the course of multilayer deposition, the nubs of the echellette substrate shadow a significant portion of the facets leading to the formation of cavities in the vicinity of the nubs - Fig. 9b. Nevertheless, a significant part of the facet looks acceptable for diffraction measurements – Fig. 9a.
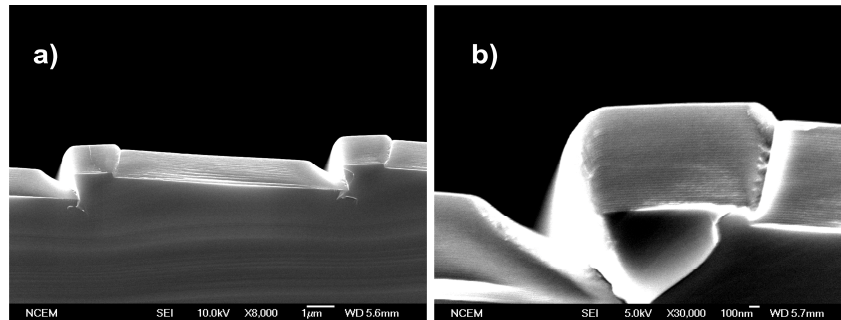

Figure 9: a) SEM image of a cross section of the Sc/Si multilayer coating deposited on an echellette grating with 10 µm period made of a CZ wafer. b) Higher magnification image of the vicinity of a groove nub. In the course of multilayer deposition, the nubs of the echellette substrate shadow a significant portion of the facets leading to formation of cavities in the vicinity of the nubs and decreasing the effective area of the multilayer coating.

The Sc/Si multilayer coating on the echellette grating was mechanically polished using a number of diamond pastes. In the course of polishing, the coating on the top of the echellette nubs was totally removed – Fig. 10. This avoids parasitic diffraction from a periodic multilayer mirror structure appearing on the top of nubs after coating.

Figure 10 shows a SEM image of the sliced multilayer grating as it looks like after the polishing is completed. The wide black strips in Fig. 10 are the surfaces of the Si nubs cleaned by the polishing. The filled light-gray strips below the Si strips are the polished material of the coating, which was deposited on the steep walls of the nubs that was not shadowed during the deposition. Resolution of the SEM is not enough to resolve the very dense layer structure of the strips.
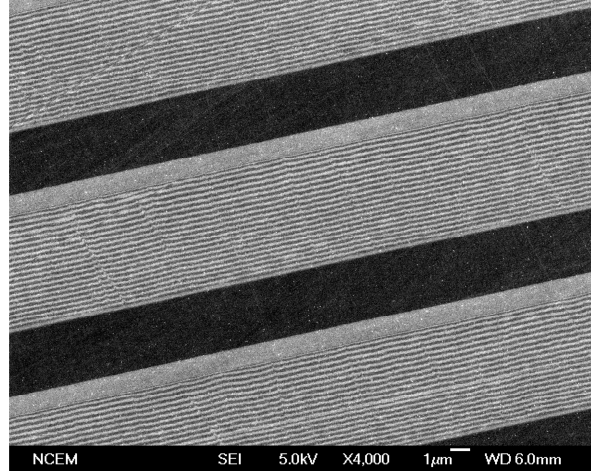
Figure 10: SEM images of the surface of the sliced Sc/Si multilayer grating prototype. The lined structure of the sliced multilayer is well visible. There is a variation of the period of the sliced multilayer lines within a multilayer stack of an echellette groove. The variation is due to the curved shape of the echellette facets. The surface roughness affects the straightness of the lines.

The periodic (with period of 10 µm determined by the echellette substrate) structures of very dense lines in Fig. 10 is the sliced multilayer grating. The period of the sliced grating is about 270 nm that corresponds to the grating groove density of about 3,700 lines per millimeter. There is a noticeable gradual variation of the line periodicity inside a 10 µm step. This is due to the curved shape of the echellette facets discussed in Sec. 2.2. The resulting useful area of the dense line structures is only about 60% of the total surface of the grating. The grating is a first proof of principle prototype fabricated according to the technology proposed.[27] The prototype with such parameters is suitable for EUV applications.

3. INVESTIGATION OF DIFFRACTION EFFICIENCY OF THE SLICED MULTILAYER GRATING PROTOTYPE

The diffraction measurements with the EUV grating prototype with sliced Sc/Si multilayer were performed at the ALS beam line BL6.3.2.[31,32] The beam line is equipped with a reflectometer capable of independently varying the angle of incidence on the sample ($\theta_s = 90$-α) and the detector angle ($\theta_d = 180$−α−β) – Fig. 11. High accuracy reflectivity and diffraction measurements are possible at wavelengths up to 50 nm.
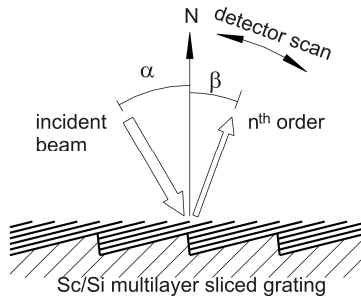

Figure 11: Geometry of the experiment at the ALS beam line BL6.3.2. to measure diffraction efficiency of the sliced Sc/Si multilayer grating prototype.

First, the witness sample coated with the same multilayer as the prototype grating was investigated.

3.1 Reflectivity of the Sc/Si multilayer

Figure 12 shows the small angle reflectivity of the Sc/Si multilayer witness deposited on a flat Si substrate. The θ-2θ scan[31] of the detector was performed at the photon wavelength of 0.154 nm (Cu$_{k\alpha1}$ edge). The high quality of the periodic multilayer stack is manifested with a set of well resolved diffraction peaks extending to the diffraction angles of 7 degrees.
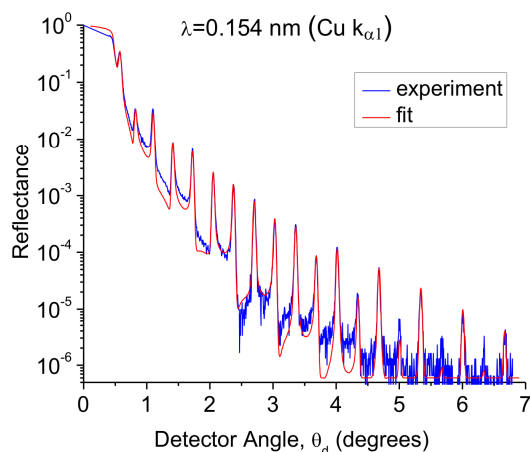
Figure 12: Reflectivity of the Sc/Si multilayer as a function of the detector angular position, θ_d. The reflectivity was measured near the Cu $K_{\alpha 1}$ edge at x-ray wavelength of 0.154 nm. The high quality of the periodic multilayer stack is shown by a set of well resolved diffraction peaks that extend to the diffraction angles of 7 degrees.

The parameters of the multilayer coating found by fitting of the experimentally measured diffractogram in Fig. 12 with a model consisting of four layers, Sc/ScSi/Si/ScSi, including two interlayer of silicide, are listed in Table 1. The normal incidence reflectivity of the witness was measured to be 44% at the photon wavelength of 46.5 nm – Fig. 13.

Table 1. Parameters of the Sc/Si multilayers determined with the small angle x-ray diffraction measurements.

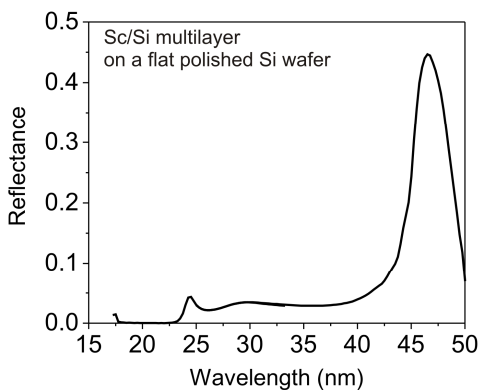| Material of a layer	ScSi	Sc	ScSi	Si
thickness of the layer, nm	2.3	9.53	2.5	12.22
interface roughness, nm	0.3	0.6	0.42	0.4

Figure 13: Reflectivity vs photon wavelength of the flat witness mirror coated with Sc/Si multilayer together with the echellette substrate. The measurement was performed at an angle of 5 degrees from normal incidence the ALS beam line 6.3.2. The maximum of mirror reflectivity of 44% is at the x-ray wavelength of 46.5 nm.

3.2 Diffraction efficiency of the sliced Sc/Si multilayer grating prototype

The diffraction efficiency measurements with the sliced Sc/Si multilayer prototype were also performed at the ALS beam line 6.3.2 – Fig. 11. In the course of the measurements, the photon wavelength was varied in the range of 43-47 nm near the position of the reflectance maximum for the multilayer mirror in Fig. 13. The incidence angle of the photon beam was adjusted to 10 degrees and was held constant; while the angle of diffraction was scanned by translating the detector.
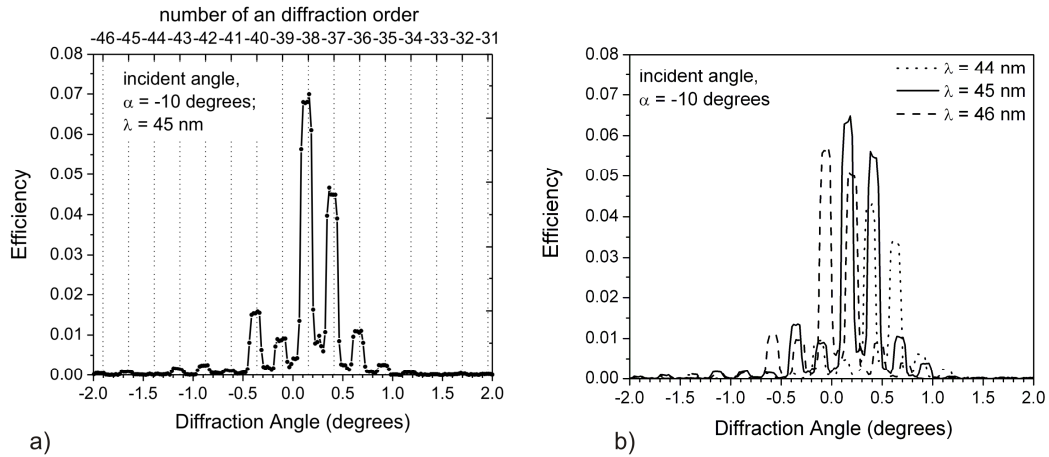
Figure 14: a) Angular dependence of the diffraction efficiency of the Sc/Si multilayer sliced grating measured at the photon wavelength of 45 nm. For reference the angular positions of the corresponding diffraction orders calculated for the grating period of 10 µm are shown as a additional scale axis on the top of the plot. b) Angular dependence of the diffraction efficiency of the prototype measured at three different photon wavelengths. The shift of the dependence is clear evidence for dispersive power of the prototype grating. The tiny difference of the profiles measured at the photon wavelength of 45 nm and presented in the plots a) and b) is due to the fact that the profiles were taken with different samples with slightly different groove period.

Figure 14 presents the diffraction profiles for the grating prototype measured at different photon energies. For each profile, there are several peaks which correspond to the high order diffraction induced by the 10-µm periodicity of lines of the sliced grating prototype. The angular width 0.12° of a diffraction peak is defined by the detector slit size of ~500 µm.

For the photon wavelength of 45 nm (Fig. 14a), an absolute efficiency of diffraction in the -38th order is ~7%. The total efficiency of the prototype evaluated by summing over all observed orders is about ~14.7%. After correction for the effective (working) surface of the grating (excluding the surfaces of the nubs), the total efficiency of the contributing surface becomes 24.5%. This is about 55% of the maximum reflectivity of the multilayer coating itself for a photon wavelength of 45 nm – Fig. 13. The dispersive power of the prototype grating is demonstrated with Fig. 14b via the shifted diffraction profiles measured at the photon wavelengths of 44, 45, and 46 nm.

The measurements in Fig. 14 indicate that the Sc/Si multilayer sliced grating prototype diffracts into multiple orders rather than diffracts to solely one (first) diffraction order, as one should expect for an ideal sliced multilayer grating. This behavior of the prototype relates to the residual 10 µm periodicity of the grating structure. The silicon nubs and the at-nubs wide strips of the coating material as well as the gradient of periodicity of the sliced multilayer lines (Fig. 10), all have the 10 µm period determined by the echellette substrate.

The gradient of periodicity of the sliced multilayer lines is probably the main reason for the approximately equal absolute diffraction efficiency for the 37th and 38th orders (Fig. 14). Indeed, due to the gradient of periodicity of the lines (curvature of the facets and, correspondingly, the multilayer), the blaze condition of the multilayer is satisfied for both these orders.

4. CONCLUSION

We have presented proof of principle results of development of a principally new method for fabrication of super dense diffraction gratings for EUV and soft x-ray applications. The peculiarities of the processes used for fabrication of a first prototype of sliced multilayer gratings optimized for photon wavelength of 45 nm have been described. We have also discussed the results of measurement of diffraction efficiency of the prototype grating. The grating has demonstrated an absolute efficiency of diffraction to the main order (that is the -38th order for the 10 µm echellette period) of ~7%. The total efficiency (evaluated by summing over all observed orders and with correction for the effective surface of the grating, excluding the surface of the nubs), is about 55% of the maximum reflectivity of the Sc/Si multilayer coating applied.

In spite of the fact that the prototype grating has already demonstrated rather high performance, it is far from an ideal sliced multilayer grating, which would be expected to diffract solely in the first order determined by a period of the sliced multilayer lines. The diffraction to multiple orders observed in the experiments with the prototype is due to residual 10 µm periodicity of the grating structure. The major distortion factor is the gradient of periodicity of the sliced multilayer lines inside one echellette groove that also repeats with the 10-µm period of the echellette substrate. The gradient of periodicity of the lines is due to the curvature of the echellette facets. We expect that the facet profile can be significantly improved by using an echellette with a smaller period and by using an etchant with a higher anisotropy of etching.

We also believe that the quality of the grating would be improve by suppression of the shadowing effect e.g., with a multilayer coating technique using a collimated ion-beam. The overall efficiency of the grating can be increased almost by a factor of two by removal of the echellette nubs e.g., with the lift-off technology described in Ref.[22]

5. ACKNOWLEDGEMENTS

DISCLAIMER

REFERENCES

[1] Kowalski, M. P., Barbee, Jr., T. W.,and Hunter, W. R., "Replication of a holographic ion-etched spherical blazed grating for use at extreme-ultraviolet wavelengths: efficiency," Appl. Opt. 45 (2), 322-334 (2006).

[2] Lin, H., Zhang, L., Li, L., Jin, Ch., Zhou, H., and Huo, T., "High-efficiency multilayer-coated ion-beam-etched blazed grating in the extreme-ultraviolet wavelength region," Opt. Lett. 33(5), 485-487 (2008).

[3] Imazono, T., Ishino, M., Koike, M., Sasai, H., and Sano, K., "Fabrication and evaluation of a wideband multilayer laminar-type holographic grating for use with a soft-x-ray flat-field spectrograph in the region of 1.7 keV," Appl. Opt. 46(28), 7054 (2007).

[4] Workshop on "Soft X-Ray Science in the Next Millennium: The Future of Photon-In/Photon-Out Experiments. (Pikeville, Tennessee March 15–18, 2000), http://www.phys.utk.edu/WPWebSite/ewp_workshop_XRay_Report.pdf.

[5] Eisebitt, S., Eberhardt, W., "Band structure information and resonant inelastic soft X-ray scattering in broad band solids," J. El. Spec. Rel. Phen. 110-111(1-3), 335-358 (2000).

[6] Kotani, A., Shin, S., "Resonant inelastic X-ray scattering spectra for electrons in solids," Rev. Mod. Phys., 73(1), 203-246 (2001).

[7] Altarelli, M., "Resonant X-ray scattering: a theoretical introduction," in: "Magnetism: A Synchrotron Radiation Approach" (Springer-Verlag. 2006), 201-242.

[8] Barbee, Jr., T. W., "Combined microstructure X-ray optics," Rev. Sci. Instrum. 60(7), 1588-1595 (1989).

[9] Warburton, W. K., "On the diffraction properties of multilayer coated plane gratings," Nucl. Instrum. Meth., A291(1-2), 278-285 (1990).

[10] Erko, A. I., Vidal, B., Vincent, P., Agafonov, Yu. A., Martynov, V. V., Roschupkin, D. V., Brunel, M., "Multilayer grating efficiency: numerical and physical experiments," Nucl. Instrum. Meth. A, 333(2-3), 599-606 (1993).

[11] Martynov, V., Vidal, B., Vincent, P., Brunel, M., Roschupkin, D. V., Agafonov, Yu., Erko, A., Yakshin, A., "Comparison of modal and differential methods for multilayer gratings," Nucl. Instrum. Meth. 339(3), 617-625 (1994).

[12] Martynov, V. V., Padmore, H. A., Yakshin, V., Agafonov, Yu. A., "Lamellar multilayer gratings with very high diffraction efficiency," Proc. SPIE 3150, 2-8 (1997).

[13] Schnopper, H. W., Van Speybroeck, L. P., Delvaille, J. P., Epstein, A., Kallne, E., Bachrach, R. Z., Dijkstra, J., Lantward, L., "Diffraction grating transmission efficiencies for XUV and soft x rays," Appl. Opt. 16(4), 1088-1091 (1977).

[14] Maystre, D., and Petit, R., "Some recent theoretical results for gratings; application for their use in the very far ultraviolet region," Nouv. Rev. Opt., 7, 165-180, (1976).

[15] Underwood, J. H., Malek, C. K., Gullikson, E. M., Krumrey, M., "Multilayer-coated echelle gratings for soft x rays and extreme ultraviolet," Rev. Sci. Instrum., 66(2), 2147-2150 (1995).

[16] Neviere, M., Montiel, F., "Soft x-ray multilayer coated echelle gratings: electromagnetic and phenomenological study," J. Opt. Soc. Am. A, 13(4), 811-818 (1996).

[17] Naulleau, P. P., Liddle, J. A., Anderson, E. H., Gullikson, E. M., Mirkarimi, P., Salmassi, F., Spiller, E., "Fabrication of high-efficiency multilayer-coated gratings for the EUV regime using e-beam patterned substrates," Opt. Comm. 229, 109-116 (2004).

[18] Levashov, V. E., Zubarev, E. N., Fedorenko, A. I., Kondratenko, V. V., Poltseva, O. V., Yulin, S. A., Struk, I. I., Vinogradov, A. V., "High throughput and resolution compact spectrograph for the 124-250A range based on MoSi2-Si sliced multilayer grating," Opt. Comm. 109, 1-4 (1994).

[19] Fechtchenko, R. M., Vinogradov, A. V., and Voronov, D. L., "Optical properties of sliced multilayer gratings," Opt. Comm. 210, 179-186 (2002).

[20] We use the term 'echellette' after other authors21 and because of a definition given in the book by E.C. Loewen and E. Popov, "Diffraction Gratings and Applications," (Marcel Dekker, Inc., 1997), p. 73.

[21] Philippe, P., Valette, S., Mendez, O. M., Maystre, D., "Wavelength demultiplexer: using echelette gratings on silicon substrate." Appl. Opt. 24(7), 1006-1011 (1985).

[22] Chang, Ch.-H., "Fabriaction of extremely Smooth Blazed Diffraction Gratings," Master Thesis (MIT, 2004).

[23] James, R. W., "The Optical Principles of the Diffraction of X-rays," London: Bell (1948).

[24] Shvyd'ko, Yu., "X-Ray Optics," Springer-Verlag (2004).

[25] Shvyd'ko, Yu. V., Lerche, M., Küetgens, U., Rüter, H. D., Alatas, A., Zhao, J., "X-Ray Bragg Diffraction in Asymmetric Backscattering Geometry," Phys. Rev. Lett., 97, p. 235502 (2006).

[26] Petersen, H., Jung, C., Hellwig, C., Peatman, W. B., and Gudat, W., "Review of plane grating focusing for soft x-ray monochromators," Rev. Sci. Instrum., 66(1), p. 1-14 (1995).

[27] Voronov, D. L., Cambie, R., Feshchenko, R. M., Gullikson, E., Padmore, H. A., Vinogradov, A. V., Yashchuk, V. V., "Development of an ultra-high resolution diffraction grating for soft X-rays," Proc. SPIE 6705, 67050E (2007).

[28] Garcia, S. P., Bao, H., Hines, M. A., "Etchant anisotropy controls the step bunching instability in KOH etching of silicon," Phys. Rev. Lett. 93(16), 166102/1-4 (2004).

[29] Nijdam, A. J., Gardeniers, J. G. E., Gui, C., Elwenspoek, M., "Etching pits and dislocations in Si {111}," Sensors and Actuators 86, 238-247 (200).

[30] Nijdam, A. J., Anisotropic wet-chemical etching of silicon pits, peaks, principles, pyramids, and particles," Ph. D. Thesis (University of Twente, Enschede, the Netherlands, 2001).

[31] Underwood, J. H., Gullikson, E. M., Koike, M., Batson, P. J., "Beamline for metrology of X-ray/EUV optics at the Advanced Light Source," Proc. SPIE 3113, 214-221 (1997).

[32] Underwood, J. H., Gullikson, E. M., Koike, M., Batson, P. J., Denham, P. E., Franck, K. D., Tackaberry, R. E., Steele, W. F., "Calibration and standards beamline 6.3.2 at the Advanced Light Source," Rev. Sci. Instrum. 67(9), 3372-3375 (1996).